Experimental Study of Swirling Flow with a Surfactant for Drag Reduction in a Pipe*

Mizue MUNEKATA**, Eiji SHIBATA***, Kazuyoshi MATSUZAKI** and Hideki OHBA**

The surfactant used in this study is well known as an additive for drag reduction in straight (non-swirling) pipe flow. This paper deals with swirling flow characteristics of a surfactant solution. We investigated the effects of surfactant concentration and Reynolds number on flow characteristics. It is shown that the drag reducing effect is less than in straight pipe flow, and that the surfactant solution must be highly concentrated with great elasticity in order to produce a drag reduction. As the results of velocity measurement by LDV and wall pressure measurement in the axial direction, it is expected that the swirl intensity of the drag reducing swirling flow with a surfactant decays more quickly as the flow progresses downstream. And we propose that this mechanism helps create the drag reduction in swirling flow. For the velocity profiles of drag reducing swirling flow, only the forced-vortex type is observed in this experiment. This suggests that the velocity profiles of drag reducing swirling flow change more quickly to a forced-vortex type from a Rankin's combined vortex type. It is also reported that turbulence intensity of drag reducing swirling flow is smaller than turbulence intensity of a solvent.

Key Words: Swirling Flow, Surfactant, Non-Newtonian Fluid, Flow Measurement, Drag Reduction, Laser Doppler Velocimeter (LDV), Pipe Flow

1. Introduction

It is well known that the addition of certain surfactants, as well as polymers, to a Newtonian fluid causes considerable drag reduction on turbulent straight pipe flow without swirl. However, the degree of this effect on swirling pipe flow is not yet known. In addition, it is very interesting to study the flow characteristics of swirling flow of a surfactant solution.

In addition to simple shear flow in a straight cylindrical pipe, studies of flow fields in a pipe with a noncircular section, such as a rectangular cross section, have been carried out[1]. The existence of a secondary flow has also been reported for non-Newtonian fluids such as dilute polymer solutions and surfactant solutions. Laminar flow and turbulent flow for Newtonian fluids in a bend with circular or rectangular cross sections have been reported in detail. For non-Newtonian fluids, the friction coefficient, the cross sectional distribution of longitudinal velocity by Laser Doppler Velocimeter (LDV)[2], and numerical simulation results obtained using the power law[3] have been reported for polymer solution flow. For surfactant solution flow, the drag reducing effect in a curved pipe has been investigated, and it has been reported that the effect decreases in comparison with the straight pipe flow[4].

Although, many investigations have been performed for non-Newtonian fluid flow, results of research on swirling pipe flow of non-Newtonian fluids have apparently not been published to date. Some investigators have studied the rotating flow of non-Newtonian fluids in a container such as a rotational viscometer. Most of the flow fields, however, are in the region of low Reynolds numbers, and the main stream has a tangential velocity. In this study, the drag reducing effect of a dilute surfactant solution in swirling pipe flow was investigated and compared with both the drag reducing effect of straight pipe flow without swirl of non-Newtonian fluids and swirling flow of Newtonian fluids. From our previous research for swirling flow of non-Newtonian fluids in a rectangular tube with an aspect ratio of 1.3, we clearly showed that the drag reducing effect was less than that of straight flow without swirl[5]. However, conclusions from this study of swirling flow in a rectangular tube were limited by the existence of a complicated secondary flow at the corners of cross sections and by using a measurement pipe that was too short to obtain useful data. To minimize unnecessary variables, the test pipe used in this

*Received on July 31, 2001.
**Kumamoto University, Kurokami 2-39-1, Kumamoto, Japan 860-8555.
***Graduate School of Kumamoto University, Kurokami 2-39-1, Kumamoto, Japan 860-8555.

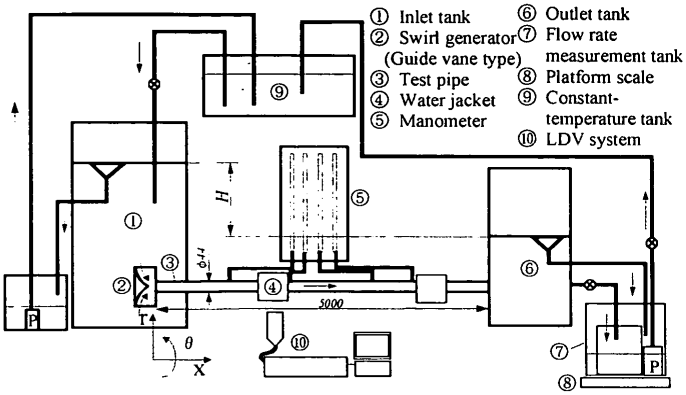

Fig. 1 Experimental setup

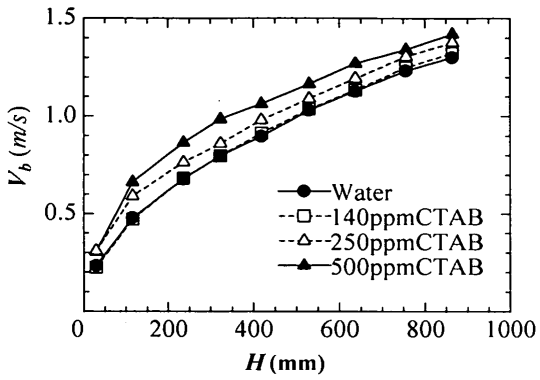

Fig.2 Bulk velocity, V_b,vs. head difference, H, at 20°C

experiment has a circular cross section and sufficient length. Moreover, in our previous setup, the generated swirling flow was not symmetrical because the swirling flow was generated by inlet flow from the rectangular hole located at non-centerline of the sidewall of the rectangular test tube. In the present setup, a guide vane type swirl generator[6] was installed upstream of the pipe, and axisymmetric swirling flow was formed upstream of pipe flow. This paper shows the effects of surfactant concentration and bulk velocity on the friction coefficient, and shows the changes of wall pressure in axial direction. Further, for drag reducing swirling flow, swirl intensity, velocity profiles and turbulence intensity profiles are shown. The LDV was used to measure velocity and turbulence intensity. The results are discussed and compared with swirling flow and straight flow of a solvent (water).

2. Experimental setup and measurement method

Figure 1 shows experimental setup. The flow is induced by solution level difference, H, between the inlet tank and the outlet tank. Two different solution levels can be kept constant by an overflow system. The swirl generator, installed at upstream of the pipe, has twelve guide vanes. The inclination angle of the vane chord was arbitrarily chosen. The inner diameter, d (=2R), and the length of the cylindrical pipe are 44 mm and 5000 mm (114d), respectively. The solution is kept at a constant temperature (± 0.5 °C) by a constant temperature tank containing cooling and heating coils.

Mass flow rate, wall pressure, and velocity were measured for nine solution level differences. Mass flow rate was measured by a platform scale. Wall pressure was measured at five axial positions and was calculated by averaging wall pressures measured from four pressure taps at equal distance in the circumferential direction. The axial and tangential components of time mean velocity and turbulence intensity were measured by LDV. Axial position, x, is defined as the distance from the inlet of the pipe, and positive tangential direction is defined as tangential direction induced by the guide vanes. Polyethylene particles with a 6 μm diameter and specific gravity of 0.918 were used as seeding particles for LDV measurements.

The surfactant solution (CTAB) used in this experiment was made with the addition of equal mole quantities of cetyl-trimetyl ammonium bromide and sodium salicylate to water. The concentrations of CTAB used in this experiment are 140, 250 and 500ppm. The concentration was determined by the weight ratio of only cetyl-trimetyl ammonium bromide to the solvent. The kinematic viscosity is characterized by "the shear-thinning property" where CTAB increases with decreasing shear rate as the concentration increases. CTAB can also be classified as a pseudo-plastic fluid in non-Newtonian fluids. A constant kinematic viscosity for CTAB could not be determined, because, in swirling flow, wall shear stress as well as axial and tangential velocity profiles over the cross section of the pipe all change in a streamwise direction. Re, therefore, was calculated using the same kinematic viscosity as water. Having elastic properties, CTAB is also a viscoelastic fluid. The higher the concentration of CTAB, the larger the elastic property or elongational viscosity of CTAB is.

3. Results and discussion

3.1 Bulk velocity and head difference

Figure 2 shows the relationship between head difference, H, and bulk velocity, V_b. At the lowest concentration, 140ppm CTAB, V_b is consistent with V_b of water for all H. At higher concentrations, 250ppm and 500ppm CTAB, however, V_b becomes larger than V_b of water. An increasing rate of V_b (IR; increasing rate of flow rate: $IR=(V_{b,CTAB}-V_{b,water})/V_{b,water}\times 100$) under the same H condition for both CTAB and water, tends to decrease with an increase in H. For the given range of H in this experiment, the maximum increasing rate of V_b is 45% when H=30mm at 500ppm CTAB. Because these values include the influence of inlet and outlet energy losses, the friction loss coefficient is calculated from wall pressure loss in order to estimate a net energy loss of swirling flow.

3.2 Friction coefficient from wall pressure loss

For swirling flow, the distribution of static pressure

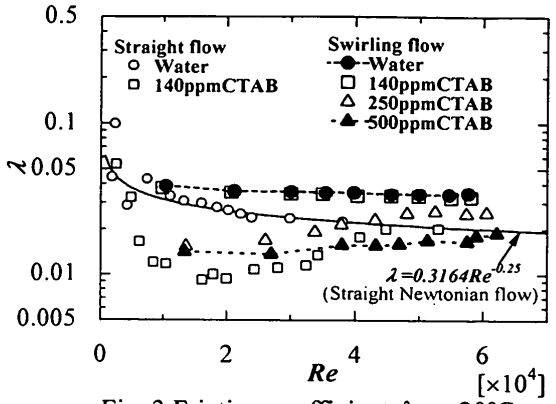

Fig. 3 Friction coefficient, λ, at 20°C

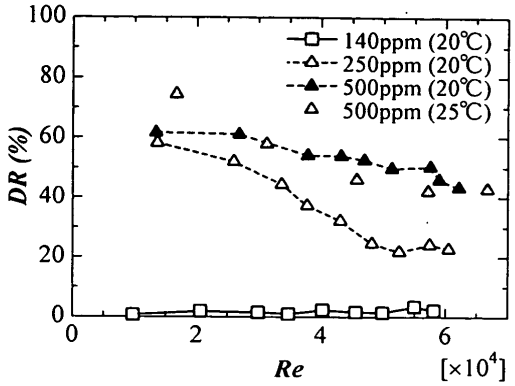

Fig.4 Drag reducing rate, DR

and total pressure is not uniform throughout the cross section of the pipe. Swirl intensity decreases as the flow moves downstream, therefore, different radial profiles in tangential and axial velocity components exists between upstream and downstream sections. As a result, theoretically, net energy loss cannot be estimated from wall pressure alone. The differences, however, between total pressure losses calculated by adding the dynamic pressure profile to the static pressure profile which was estimated from the tangential velocity profile and wall pressure, and pressure losses obtained from wall pressure only, are negligible. The friction coefficient for the purpose of this study, therefore, was calculated for wall pressure only.

Figure 3 shows the relationship between the friction coefficient and Reynolds number; the total pressure losses are the wall pressure difference between two positions separated by 51 times the pipe inner diameter. The data for straight shear flow (non-swirling flow) are also shown in Figure 3. The friction coefficient for water is consistent with Blasius's equation for Newtonian fluid flow. At Reynolds numbers less than 4×10^4 for straight flow of 140ppm CTAB, drag reduction is remarkable. However the 140ppm CTAB data is consistent with Blasius's equation when Reynolds numbers above 4×10^4; there was no drag reduction. This reason is considered as follows: when the excessive shear stress acts on the shear layer, the elastic stress by the surfactant is not effective. The energy of strain by the excessive shear stress cannot kept in the fluid. Therefore, the energy is dissipated, and the CTAB solution flow begins to behave as Newtonian fluid flow.

There is no drag reduction in 140ppm CTAB swirling flow; the friction coefficients of water and 140ppm CTAB are similar and are larger than the friction coefficients in straight Newtonian fluid flow. In straight flow, it has been confirmed that the drag reduction rate increases with increasing CTAB concentrations up to a certain concentration. Therefore, 250ppm and 500ppm CTAB were also tested in this experiment. The friction coefficients of 250ppm and 500ppm CTAB in swirling flow are lower than those of water, thus when the concentration of CTAB is high, significant drag reduction occurs. If the effect of drag reduction is due to the elasticity of CTAB, then the elasticity of CTAB when the concentration is low, is too small to observe any drag reduction.

For water and 140ppm CTAB, the friction coefficients decrease slightly with an increase in Reynolds number within the limits of this experiment; but for 250ppm and 500ppm, the friction coefficients tend to increase with an increase in Reynolds number.

3.3 Drag reducing rate

Drag reducing rate (DR) is defined by:

$$DR(\%)=\left(\frac{\lambda_W-\lambda_D}{\lambda_W}\right)\times100 \quad \cdots\cdots (1)$$

Here, λ_D is the friction coefficient of the surfactant solution, and λ_w is the friction coefficient of water at a given Reynolds number for the surfactant solution. The λ_w is estimated by following equation:

$$\lambda_W = 0.0725\,\mathrm{Re}^{-0.071} \quad \cdots\cdots (2)$$

DR is shown as a function of Reynolds number in Figure 4. DR for 140ppm CTAB is almost zero percent; but for 250ppm and 500ppm CTAB, a maximum DR of 60~75% was obtained. For both 250ppm and 500ppm CTAB, DR decreases with an increase in Reynolds number, but DR of 250ppm CTAB decreases more rapidly than 500ppm CTAB. Consequently, we assume that when the concentration of CTAB is higher than 500ppm, DR at high Reynolds numbers may increase with an increase in the concentration but the increase in the maximum DR will be relatively small.

3.4 Profile of wall pressure along the pipe axis

The wall pressure coefficient, Cp, is defined by following equation:

$$Cp=\left(P_W-P_{ref}\right)/\left(\rho V_b^2/2\right) \quad \cdots\cdots (3)$$

Here P_w and P_{ref} are the wall pressures at each measurement position and at a reference position where x/d=24.9, respectively. Figure 5 shows Cp distribution in the axial direction where H=160mm. Similar distributions were also obtained for other H values. The Cp distribution for straight flow of Newtonian fluids, fitted using Darcy-Weisbach's equation and Blasius's equation, has a slope $-\lambda=-0.3164/\mathrm{Re}^{0.25}$. Both 250ppm

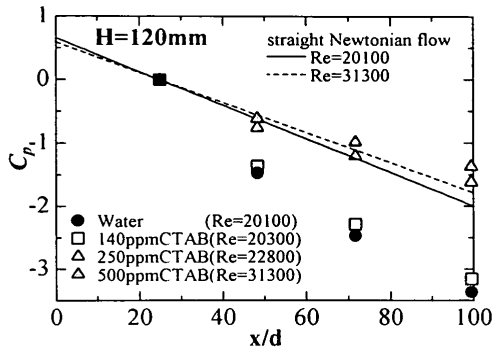

Fig. 5 Wall pressure coefficient at H=120mm

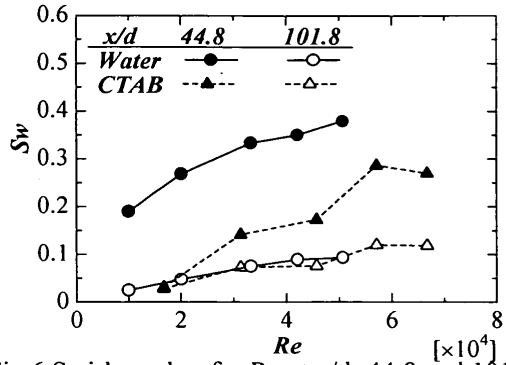

Fig.6 Swirl number for Re at x/d=44.8 and 101.8

and 500ppm CTAB have less pressure loss than straight flow of Newtonian fluids, as their slopes are less than $-0.3164/Re^{0.25}$. Further, the Cp profile of fully developed straight pipe flow is straight, yet, the Cp profile of swirling flow has curvature. It was expected that the swirl intensity would decrease downstream. It was also expected that a decrease in swirl intensity of water and 140ppm CTAB would be larger than in 250ppm or 500ppm CTAB downstream of x/d=24.9, since the former curvature is larger than the latter one.

3.5 Swirl intensity

Swirl intensity can be presented by swirl number, Sw, as follows[7]:

$$Sw = \frac{\int_0^R V_x(r) V_\theta(r) r^2 \, dr}{R \int_0^R V_x(r)^2 r \, dr} \quad \cdots\cdots (4)$$

Here V_x and V_θ are axial and tangential velocity, respectively, and are measured by LDV. Since swirl flow is generally non-axisymmetric flow, V_x and V_θ are measured crosswise throughout the cross section of the pipe in order to obtain an accurate swirl number. Thus, Sw is obtained by averaging four values for Sw. The relationship between Sw and Re at x/d=44.8 and 101.8 is shown in Figure 6. Because differences of Sw between x/d=44.8 and 101.8 for 500ppm is less than for water, the decay of Sw for 500ppm CTAB is smaller than for water. At the downstream cross section, x/d=101.8, however, both 500ppm CTAB and water have equivalent values. This means that the profiles of the swirl decay are different from each other. If it is assumed that the initial swirl intensities just behind the guide vanes are equivalent at the same Re for both 500ppm CTAB and water, the upstream decay of Sw for 500ppm CTAB occurs more quickly than for water. The quick decay of Sw is thought to be due to a centrifugal effect that is suppressed by the elasticity of CTAB.

In all cases Sw tends to increase with increasing Re up to some Re. This indicates that Sw decreases more quickly at a low Re. As a result, Sw at a low Re is smaller for the same cross section. This tendency is consistent with other reports[8].

3.6 Velocity profile

LDV measurements were taken for flow conditions summarized in Table 1. Figures 7 and 8 show time mean-velocity profiles, which were obtained by taking measurements along the horizontal and vertical line through the center of the pipe at x/d=44.8 and 101.8. Tangential velocity V_θ of water at x/d=44.8 has a pure forced-free vortex typed profile (a Rankin's combined vortex model), as shown in Fig.7 (a2). The V_θ profile has three regions, which are core, annular, and wall as reported in detail by Kitoh (1991)[8]. The annular and core regions exhibit free and forced-vortex type profiles, respectively. The same three regions are also seen in the profiles of axial velocity, V_x. The extent of each vortex region changes in accordance with the swirl intensity as shown in Fig.7 (a1),(a2). It is similar to the Kitoh's results[8]. Minimum V_x at the core region becomes smaller as the flow rate or Sw increases, and reverse flow is observed for W760 and W530. The reverse flow is caused by an adverse pressure gradient formed in the center of the pipe by the decay of swirl intensity in the downstream direction. Maximum V_θ becomes larger with an increase in Re(Fig.7(a2)). An increase in maximum V_θ corresponds to an increase in Sw for the same location of cross section.

Figures 7(b1) and (b2) show the velocity profiles at x/d=44.8 for 500ppm CTAB. The V_x and V_θ profiles have no core regions in all cases. Contrary to the profiles for water, the values of V_x in the central part of the pipe become slightly higher as Re increases, except for the case of C30. The V_x profile of C30 has a bell-type curve such as seen for a laminar pipe flow. The V_θ profile in Fig.7 (b2) is similar to a forced-vortex type profile except for the near wall region.

The Sw at the downstream cross section, x/d=101.8, is smaller than at x/d=44.8, and the core region cannot be observed clearly in Figure 8. Though V_x profiles of water at high Re are fairly low near the swirl center, all V_θ profiles of water and 500ppm CTAB (Figs.8 (a2),(b2)) are forced-vortex types. The V_x profiles of C30 at both x/d=44.8 and 101.8 are different from the other profiles.

As it is reasonable that the velocity distribution depends on the swirl intensity, next the difference between profiles of water and 500ppm CTAB at the same swirl intensity, Sw=0.27, is discussed. The velocity profile of W120 at x/d=44.8 has the Rankin's combined vortex type, but the profile of C760 at x/d=44.8 has the

Table 1 Flow conditions of LDV measurements

H (mm)	Symbol	Water (20 °C)					500ppm CTAB (25°C)						
		Abbre-viation	V_b (m/s)	Re	Sw x/d =44.8	Sw x/d =101.8	Abbre-viation	V_b (m/s)	Re	Sw x/d =44.8	Sw x/d =101.8	DR (%)	IR (%)
30	□	**W30**	0.229	10000	0.190	0.025	**C30**	0.339	16700	0.031	0.028	74.5	44.9
120	▲	**W120**	0.458	20100	0.269	0.048	**C120**	0.636	31300	0.142	0.073	57.9	38.6
320	△	**W320**	0.758	33300	0.334	0.075	**C320**	0.926	45700	0.173	0.076	46.0	22.3
530	●	**W530**	0.952	42100	0.351	0.089	**C530**	1.147	57100	0.287	0.112	42.1	20.4
760	○	**W760**	1.140	50700	0.380	0.096	**C760**	1.338	66700	0.270	0.119	42.8	14.8

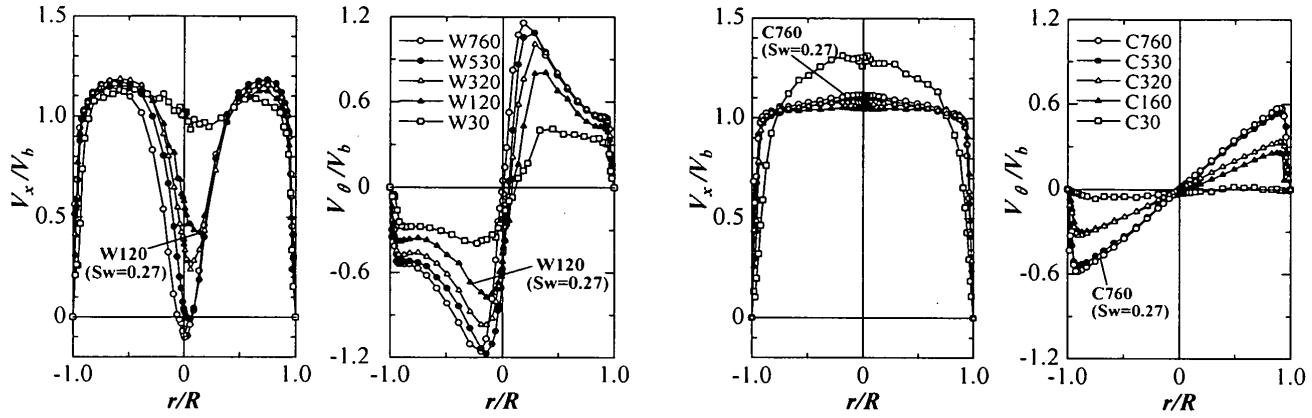

(a1) V_x of Water (a2) V_θ of Water (b1) V_x of 500ppm CTAB (b2) V_θ of 500ppm CTAB

Fig. 7 Distributions of V_x and V_θ at x/d=44.8; flow properties are presented in Table1.

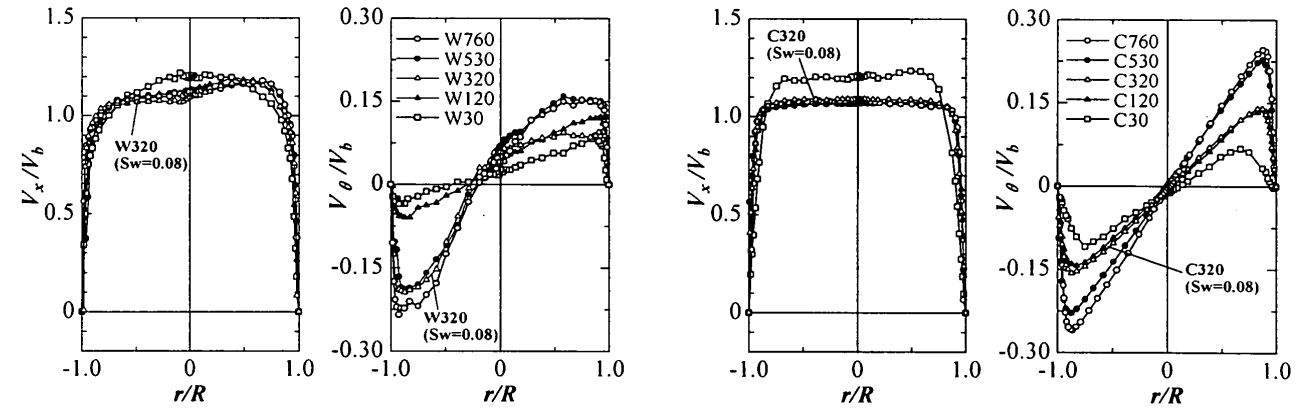

(a1) V_x of Water (a2) V_θ of Water (b1) V_x of 500ppm CTAB (b2) V_θ of 500ppm CTAB

Fig. 8 Distributions of V_x and V_θ at x/d=101.8; flow properties are presented in Table1.

forced-vortex type. When Sw=0.08, both 500ppm CTAB and water have the forced-vortex type profile, in comparison between C320 and W320 at x/d=101.8. Similar tends are obtained for a given flow rate in both upstream and downstream section. The velocity profile just behind of guide vane has not yet been measured, but if the profile is the same for both 500ppm CTAB and water for a given flow rate, then it is thought that 500ppm CTAB would change more quickly to the forced vortex type from the Rankin's combined vortex type because of the elasticity of CTAB.

3.6 Turbulence intensity

Figures 9 show turbulence intensity, which is the root mean square (rms) of velocity fluctuations at x/d=44.8 and 101.8. In Figure 9 (a1), the rms of V_x at x/d=44.8 in water is high in the core region and the wall region, and also tends to be higher as the flow rate increases. The rms profiles have two peaks near the center of the pipe, which become more defined as the flow rate increases. It is known that those peaks

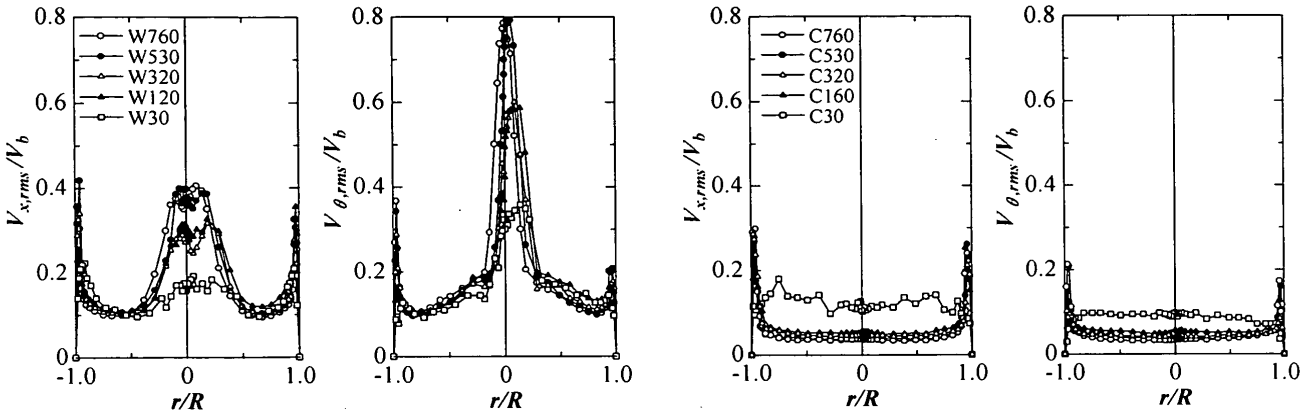

(a1) $V_{x,rms}$ of Water (a2) $V_{\theta,rms}$ of Water (b1) $V_{x,rms}$ of 500ppm CTAB (b2) $V_{\theta,rms}$ of 500ppm CTAB

Fig. 9 Distributions of Turbulence intensity $V_{x,rms}$ and $V_{\theta,rms}$ at x/d=44.8; flow properties are presented in Table1.

correspond to a maximum rms of $\partial V_\theta/\partial \xi$. Where ξ is radial distance of a coordinate with the center of the swirl as its origin. The rms of V_θ also has high turbulence in the core region and the wall region. In the core region, the rms profile of V_θ is sharp and the rms values are larger than those of V_x. On the other hand, the turbulence intensities of 500ppm CTAB at x/d=44.8 are extremely low compared with those of water (Figs. 9(b1) and (b2)). Since the velocity profiles of 500ppm CTAB have no core region, the rms profiles also have no peak near the center of the pipe. In the near-wall region, the peak tends to be larger as flow rate increases. The turbulence intensity profile of water at x/d=101.8 is similar to 500ppm CTAB at x/d=44.8. But the turbulence intensity of water at x/d=101.8 is larger than 500ppm CTAB at x/d=44.8. Further, the turbulence intensity profiles of 500ppm CTAB differ little between the upstream region, x/d=44.8, and the downstream region, x/d=101.8. Therefore, the effect of the velocity profile on the turbulence intensity is thought to be stronger than the effect of flow rate. In general, the turbulence intensity of drag reducing swirling flow with CTAB is small compared with the turbulence intensity of water given the same flow rate. It is considered that the striking difference of turbulence intensity between 500ppm CTAB and water is caused by the elasticity of CTAB.

4. Conclusions

From the results of our experiments, the following conclusions are made:

(1) The drag reducing effect for swirling flow with a surfactant is less than the drag reducing effect for straight pipe flow with a surfactant, and only a surfactant solution with a high concentration, thus high elasticity, produces drag reduction.

(2) The drag reducing effect of swirling flow decreases at higher Re.

(3) The change of Sw and wall pressure in the downstream direction is different between water and drag reducing surfactant solution. For the conditions set in this experiment, the change of drag reducing solution is smaller than that of water.

(4) The existence of drag reduction in swirling flow might be because swirl decays quickly behind the guide vanes.

(5) The velocity profiles of drag reducing swirling flow change more quickly from a Rankin's combined vortex type to a forced-vortex type.

(6) The turbulence intensity of drag reducing swirling flow is much smaller than the turbulence intensity of Newtonian swirling flow.

Acknowledgements

This work was partially supported by Grants-in-Aid for Scientific Research, No. 11210123, 12750829, from Japan Society for the Promotion Science.

References

(1) Townsend, P., Walters, K., and Waterhouse, W. M., *J. Non-Newtonian Fluid Mech.*, **1**(1946), 107-123.

(2) Takami, T., Sudou, K. and Tomita, Y., Trans. *Jpn. Soc. Mech. Eng.*, (in Japanese), **52**-475, B (1986), 1228-1242.

(3) Sugiyama, H., Akiyama, M. and Koide N., *Trans. Jpn. Soc. Mech. Eng.*, (in Japanese), **65**-633, B (1999), 1505-1512.

(4) Inaba, H, Haruki, N. and Horibe, A., Trans. *Jpn. Soc. Mech. Eng.*, (in Japanese), **66**-647, B (2000), 1818-1825.

(5) Munekata, M., Matuszaki, K. and Ohba, H., *Proceedings of Fluid Engineering Conference 2000*, (in Japanese), No.00-14 (2000), 169.

(6) Kito, O. and Suzuki, Y., Trans. *Jpn. Soc. Mech. Eng.*, (in Japanese), **51**-471, B (1985), 3461-3362.

(7) Yajnik, K. S. and Subbaiah, M. V., *J. Fluid Mech.*, **60**(1973), 665-687.

(8) Kitoh, O., *J. Fluid Mech.*, **225**(1991), 445-479.